Journal of Physics: Conference Series **568** (2014) 032012 doi:10.1088/1742-6596/568/3/032012

A calculable and correlation-based magnetic field fluctuation thermometer

A Kirste, M Regin, J Engert, D Drung and T Schurig

Physikalisch-Technische Bundesanstalt (PTB), Abbestr. 2-12, 10587 Berlin, Germany

E-mail: alexander.kirste@ptb.de

Abstract. We have developed a new Magnetic Field Fluctuation Thermometer (MFFT) specifically designed for operation in primary mode, which requires the determination of the relation between thermal flux noise density and thermodynamic temperature. The noise thermometer combines a correlation-based SQUID readout and an integrated conductivity measurement on the metallic temperature sensor with an in situ flux calibration. The operation of the MFFT is modelled theoretically. First temperature measurements in secondary mode between 9 mK and 4.2 K showed excellent agreement with a copy of the PLTS-2000 within 0.5%.

1. Introduction

The magnetic field fluctuation thermometer (MFFT) is a special variation of noise thermometry, which has found application from the highest to the lowest temperatures [1]. The MFFT exploits the fact that thermally activated noise currents inside a conductor generate fluctuating magnetic fields above its surface, which can be detected by means of a Superconducting Quantum Interference Device (SQUID) and used as a measure of the conductor's temperature [2]. The noise signals are detected as thermal magnetic flux noise (TMFN) using dc SQUID based magnetometers or gradiometers. The power spectral density (PSD) S_Φ of the TMFN exhibits a low-pass like shape and depends on the geometries of both the conductor and the detection coil as well as on the electrical conductivity of the conductor. All these properties enter into the complex impedance $Z(f)$ of the detection coil that interacts with the metallic temperature sensor. The PSD of the TMFN as measured by the detection coil at temperature T is then given by [3]:

$$S_\Phi(f,T) = \frac{4k_B T \mathrm{Re}(Z(f))}{(2\pi f)^2}, \quad (1)$$

where k_B is the Boltzmann constant and f is the frequency. The application of a MFFT for temperature measurement is based on two additional assumptions: (i) the electrical conductivity of the conductor is assumed to be constant in the considered temperature range and (ii) the geometry of the conductor-detector set-up is fixed. Then, the values for the PSD are proportional to temperature for any frequency.

While MFFTs can be made up of wire-wound coils connected to SQUID current sensors [2], [4], PTB has mainly developed MFFTs with multiloop SQUID gradiometers on a single chip [5], [6], [7]. As these MFFTs basically measure ratios of temperature by measuring ratios of noise power a calibration is required at a known reference temperature, i.e. they are operated in secondary mode.

For application of a MFFT in primary mode (pMFFT) one has to relate the measured TMFN directly to thermodynamic temperature. This was achieved by designing temperature sensor and detection coils with plain geometries to allow an easy determination of all relevant dimensions and an efficient calculation of the TMFN. In addition, the pMFFT can perform in situ measurements of the electrical conductivity of the temperature sensor and of the flux-to-voltage transfer coefficient of the SQUID gradiometer detecting the TMFN. Thus, the new pMFFT permits direct measurements of temperature in a wide range without the need for calibration at a known reference temperature.

2. Design of the pMFFT and theory of operation

The new pMFFT comprises four main parts: a metallic noise temperature sensor, a system of two gradiometric detection coils read out by two separate SQUID current sensors, a room temperature electronics to read out the SQUID sensors and a calibration coil. For the particular temperature range of the PLTS-2000 we have designed a compact device, in which the SQUID sensors are placed close to the detection coils and are thus integrated in the metallic body of the temperature sensor.

2.1. Cross-correlation technique

In order to minimize the influence of non-thermal noise sources on the measurement of the TMFN and, finally, on the measured temperature a cross-correlation technique is applied in the pMFFT similar to [4]. The suppression of the non-thermal noise is possible because these noise components occur basically uncorrelated in the two SQUID channels.

Aiming at a large signal from the TMFN the correlation must be large. This is achieved if the detection coils of the two channels are as similar as possible and sense the same volume part of the temperature sensor. The design of the detection coils is optimized to obtain almost complete correlation for the TMFN while the magnetic coupling between both channels is minimized. The proper function of the correlation technique is checked by a zero measurement without temperature sensor.

If we consider two stochastic processes $x(t)$ and $y(t)$, we can define the cross-power spectral density (CPSD) $S_{xy}(f)$ as cross-covariance between the complex Fourier amplitudes $X(f)$ and $Y(f)$. The various methods for the estimation of the PSD can be applied to estimate the CPSD. For example, the multitaper spectral estimate of the CPSD is obtained similarly to that of the PSD,

$$\hat{S}_{xy}(f) \propto \frac{1}{K}\sum_k X_k(f) Y_k^*(f) \ , \qquad (2)$$

where K is the number of tapers. The CPSD is in general a complex function with amplitude and phase. The CPSD can be normalized with the square roots of the two PSDs, $\sqrt{S_x}$ and $\sqrt{S_y}$, giving the coherency $C_{xy}(f) = S_{xy}(f)/\sqrt{S_x(f)S_y(f)}$ as normalized measure of association. For all evaluations containing the CPSD or derived expressions, we will only use the real part of the corresponding quantities. This is to avoid the inclusion of (product) terms, which do not contribute to a correlation carried out in the time domain, and would not normally contribute to a correlation carried out in the frequency domain [8].

2.2. Block diagram and theory of operation

Figure 1 shows the schematic diagram of the correlation-based pMFFT. There are two detection coils located on one Si chip, which are individually read out by two SQUID current sensors. Each SQUID sensor is connected to a flux-locked loop (FLL) electronics at room temperature. The output voltages of both channels are simultaneously read out by a spectrum analyzer.

A calibration coil, located on a second Si chip, is placed on the opposite side of the temperature sensor. The shape of this coil is similar to that of the detection coils, so that a calculable flux can be produced in the detection coils by feeding a known (dc or ac) current into the calibration coil. In the dc case, this coil is used to determine the relation between magnetic flux in the detection coils and the output voltage of the SQUID electronics. In the ac case it is used to determine the electrical conductivity of the temperature sensor.

For the measurement of magnetic flux the SQUIDs are operated in FLL mode. By using PTB SQUID current sensors [9] there are two ways to form the feedback loop for FLL operation. The common feedback directly into the SQUID (gray current path in figure 1) functions independently of the properties of the input circuit but has the disadvantage that the flux transfer from the detection coils into the SQUID becomes frequency dependent. The reason is the frequency dependent inductance of the detection coil due to the skin effect in the temperature sensor, affecting the total inductance of the input circuit. As the SQUID input circuit is superconducting, feedback can also be applied to it by means of the integrated feedback transformer. This feedback scheme has the advantage that interaction between both detection coils and between detection coils and temperature sensor is suppressed within the FLL bandwidth. Hence this FLL scheme is favored for the pMFFT.

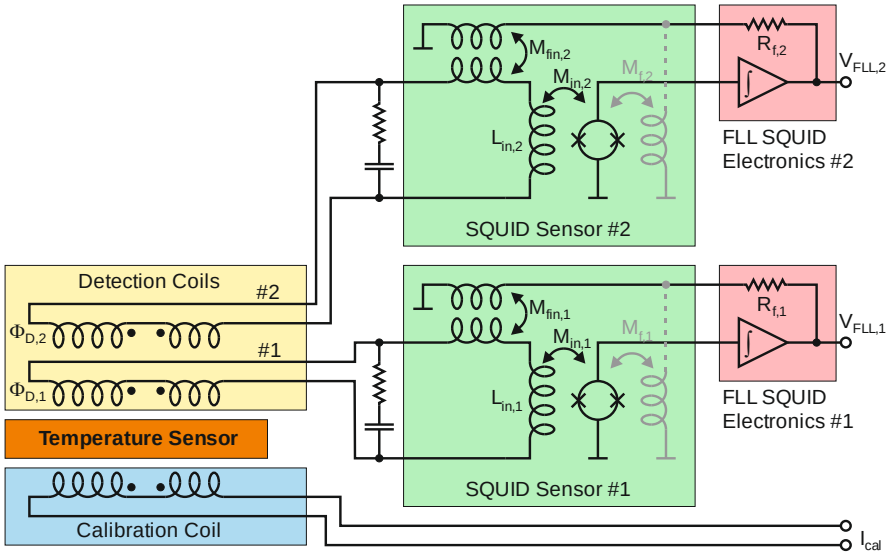

Figure 1. Schematic of the correlation-based pMFFT readout. The feedback (via M_{fin}) is into the superconducting detection coils using the feedback transformer integrated in the SQUID sensors. An alternative feedback path (gray colour) into the SQUID inductance is available for test purposes.

2.3. Theoretical model for the pMFFT and design calculations

In [10] the PSD S_Φ was calculated that is caused by the TMFN of an infinite conducting slab in a detection coil of contour c. Simplifications were possible for planar contours parallel to the slab, i.e. if $c = c(x, y, z)$ is at constant height z above the surface of the slab. We have extended this approach to calculate the CPSD caused by the TMFN in a system of two planar coils, c_1 and c_2. Following [10] we obtain

$$S_{12} \triangleq S_\Phi(c_1, c_2) = \mu^2 \sigma k_B T \iint_{-\infty}^{\infty} I_A \mathrm{e}^{-\sqrt{a^2+b^2}(z_1+z_2)} \left(I_x(c_1) I_x^*(c_2) + I_y(c_1) I_y^*(c_2)\right) \mathrm{d}a\mathrm{d}b \qquad (3)$$

with

$$I_x(c_j) = \oint_{c_j} \mathrm{e}^{\mathrm{i}ax_j} \mathrm{e}^{\mathrm{i}by_j} \mathrm{d}x_j, \quad I_y(c_j) = \oint_{c_j} \mathrm{e}^{\mathrm{i}ax_j} \mathrm{e}^{\mathrm{i}by_j} \mathrm{d}y_j, \quad j = 1, 2 \qquad (4)$$

$$I_A = \int_0^t |A(a,b)|^2 dz', \quad A(a,b) = \mathrm{e}^{-\rho' z'} (\pi\rho')^{-1} (u + v\mathrm{e}^{-2\rho'(t-z')})(u^2 - v^2 \mathrm{e}^{-2\rho' t})^{-1}, \qquad (5)$$

$$\rho^2 = a^2 + b^2, \quad \rho'^2 = \rho^2 + k^2, \quad u = 1 + \frac{\rho}{\rho'}, \quad v = 1 - \frac{\rho}{\rho'}, \quad k^2 = \mathrm{i}\mu\sigma\omega, \quad \omega = 2\pi f\,. \qquad (6)$$

Accordingly, z_j, ($j = 1, 2$) is the height of the contour c_j above the surface of the conducting slab, which has the electrical conductivity σ, magnetic permeability μ and a thickness of t. The integral I_A describes the eddy current distribution in the slab, whereas the geometry of the contours c_j is completely contained in the path integrals $I_x(c_j)$ and $I_y(c_j)$. For $c_1 = c_2$ the CPSD (3) is equal to the PSD derived in [10]. While S_{12} is generally complex its real part, $\mathrm{Re}(S_{12})$, contains the desired CPSD.

Strictly speaking, this model is valid only for a conductor of infinite size. However, the deviations of the PSD or CPSD for real conductor geometries are made very small by proper design of the detection coils. This requires that the slab overlaps the detection coils by a few times of their characteristic size (e.g. coil radius), while this condition is further relaxed for gradiometric detection coils. The approximation of a filamentary (and superconducting) coil conductor is justified if the line width of the coil conductor is small compared to all other relevant distances (e.g. coil radius, distance to the slab, gap between coil conductors). However, for an exact calculation of the deviations a comparison with FEM calculations in 2D or 3D is necessary.

The in situ determination of the electrical conductivity σ of the temperature sensor is based on the skin effect within the conductor. In the pMFFT the frequency dependence of the penetrated flux through the temperature sensor as picked up by the detection coils is measured (figure 1), where the conductivity enters via the product $\mu\sigma f$. An analytical solution for this problem is available for systems of filamentary, concentric, circular coils parallel to an infinite slab [11], [12]. This model can only be an approximation of real geometries, but the resulting deviations for σ can be made very small, requiring the same conditions as given above for the calculation of the CPSD.

Performing the same measurement with a known dc current ($f = 0$) through the calibration coil allows to calibrate both SQUID gradiometers in terms of FLL voltage ($V_{\mathrm{FLL},j}$) per magnetic flux ($\Phi_{\mathrm{D},j}$) in the detection coils ($j = 1, 2$) using calculated mutual inductances between calibration coil and detection coils.

2.4. Mechanical construction and sensor material

Figure 2 shows an inside view of the assembled pMFFT. The basic shape of the device is a cylinder with a diameter of 18 mm and a length of 100 mm. The whole body is made from high-purity copper of nominal 99.9998% purity [13]. We have determined a residual resistivity ratio of RRR ≈ 103. The cylinder has large openings from opposite sides. From one side, it takes up the Si chip with the detection coils surrounded by the two SQUID chips glued onto chip carriers (PCBs). The Si chip with the calibration coil together with another PCB is mounted on the opposite side at a fixed distance in parallel to the detection coils with the temperature sensor in between.

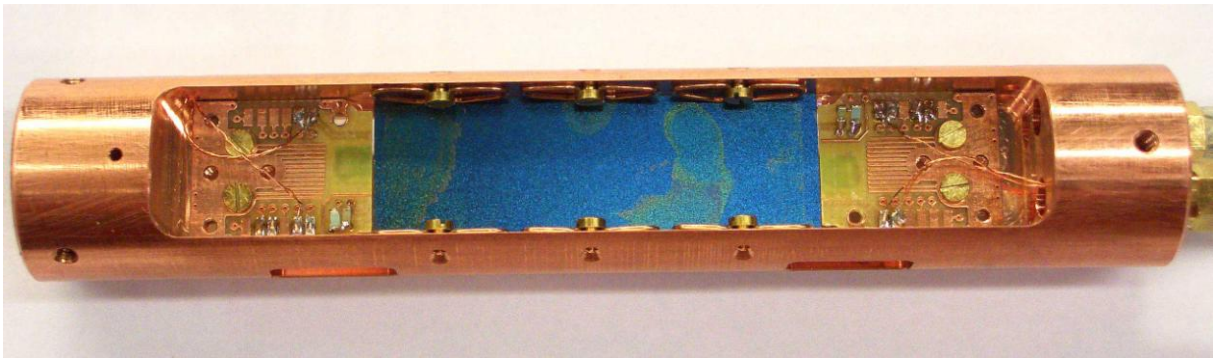

Figure 2. Inside view of the pMFFT with the magnetic shielding removed. The two SQUID current sensors are placed on PCBs directly besides the central Si chip with the detection coils. They can be seen as a shadow through the PCBs.

Only a central part near the cylinder axis serves as actual temperature sensor. This part has a thickness of about 2 mm and is virtually defined by the detection coils. In order to allow an arbitrary and minimal gap (≈50 µm or ≈100 µm depending on the side) between detection coils and temperature sensor, the Si chips are mounted face down. While the PCBs are fixed by screws, small springs (CuSn6) press the Si chips towards the edge guides providing always a proper alignment. No glue is needed to fix the coil chips. Magnetic shielding of the thermometer's inner volume is provided by an outer Nb tube, which can be removed to both sides.

2.5. Thin-film coil assemblies and SQUID sensors

Both the detection coils and the calibration coil are realized as planar thin-film coils fabricated on Si wafers using PTB's standard Nb thin-film technology. Due to the photolithography the coils can be manufactured with (sub-)micrometer precision, which is advantageous for modeling if they are mounted at distances of about 50 µm or 100 µm above the surface of the temperature sensor.

All coils are designed as series gradiometers using only a fraction of the available chip area. Despite the fact that series-parallel gradiometers with multiple degrees of freedom could couple more noise energy into the SQUID than series gradiometers with single degree of freedom, they are disadvantageous in some aspects. In particular, the calculation of the PSD of the TMFN can become more difficult and the interaction with the environment during FLL operation is not always suppressed (see section 2.2).

When designing the detection coils three properties were taken into consideration: (i) minimized capacitive coupling between both coils to avoid unnecessary interaction between the SQUIDs, (ii) maximum correlation of the TMFN from both coils to obtain a large CPSD signal or to allow an approximation of the CPSD by the single PSDs, (iii) simple coil geometries to allow simplified calculations of the TMFN and the electrical conductivity as described in section 2.3.

We have designed four different detection coils by combining different shapes (coaxial, circular or second-order gradiometers) with different arrangements formed by both coils (stripline or coplanar). For the first experiments we selected a coaxial, circular gradiometer with coplanar arrangement of both coils. The radius of the outer turns is ≈2.0 mm, eight inner turns have a radius of around 0.7 mm. In comparison with that, the distance between coil center and side walls of the temperature sensor is 6.5 mm. Line width and minimum gaps between the coils are 2.5 µm. With an estimated total coil inductance of ≈400 nH, we chose SQUID current sensors with an input inductance of 400 nH (PTB single-stage, double-transformer SQUIDs [9] of size "L") for the readout.

The SQUID sensors are glued on PCBs and mounted with sufficient distance to the conducting sensor body. Since the bond loops of the chip-to-chip connections cannot be made arbitrarily small (typical length/height 1 mm), their influence must be made sufficiently small. Depending on the detection coil this is solved either by incorporating the interconnections into a fully gradiometric design or by a large distance to the detection coils.

3. Measurements

3.1. Noise measurements with and without temperature sensor

To ensure the proper function of the cross-correlation technique, we have performed reference measurements without the temperature sensor. This was done by mounting the chip with the detection coils and the SQUID sensors on a non-metallic platform and measuring the intrinsic noise and the cross-correlation at 4.2 K. The results, referring to the flux noise in the SQUIDs, are given in figure 3. The single-channel white noise corresponds to $1.3 \cdot 10^{-6}\ \Phi_0/\mathrm{Hz}^{1/2}$, which is slightly increased compared to the intrinsic noise without input coil. An electronics noise contribution as well as $1/f$ noise are visible in the single-channel noise spectra below 100 Hz and 10 Hz, respectively. An inspection of the CPSD reveals that both channels are uncorrelated to a level of $\leq 10^{-7}\ \Phi_0/\mathrm{Hz}^{1/2}$ (after ≈98000 averages) except at the mains frequency (50 Hz) and harmonics.

Figure 4 shows the CPSD of the TMFN at 4.23 K after integration of the temperature sensor. The calculated CPSD according to (3)-(6) is based on the parameter set $z_1 = z_2 = 51.5$ µm, $1/\sigma = (1.67 \cdot 10^{-8} / 103)\ \Omega\mathrm{m}$, $t = 2.00$ mm, which is close to the independently determined values. As the originally intended calibration of the pMFFT necessary for primary thermometer mode could not be carried out, we had to measure instead the FLL parameters ($R_{\mathrm{f},j}$ and $1/M_{\mathrm{fin},j}$, $j = 1, 2$) and the flux transfer coefficients depending on the inductances in the SQUID input circuits. There is good agreement between experimental and calculated data.

In addition, we have examined the magnetic shielding of the MFFT, which reduces the influence of external magnetic fields onto the CPSD. Sensitivities exceed 310 $\mu\mathrm{T}/\Phi_0$ in dc fields for a 130 mm long

shield. Even higher shielding can be expected for ac fields due to the additional skin effect in the end sections of the sensor body.

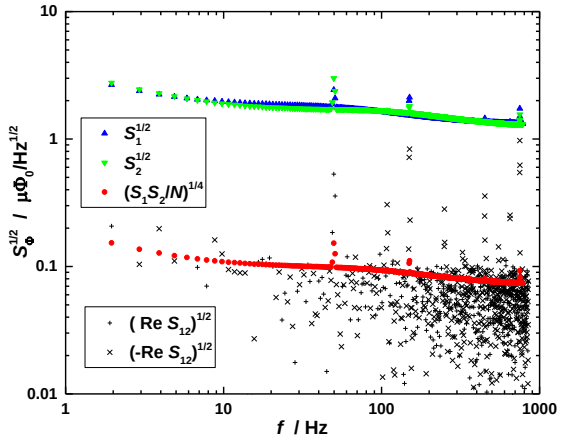

Figure 3. Flux noise referring to the SQUIDs at 4.2 K without temperature sensor. The CPSD comprises $N \approx 98000$ averages.

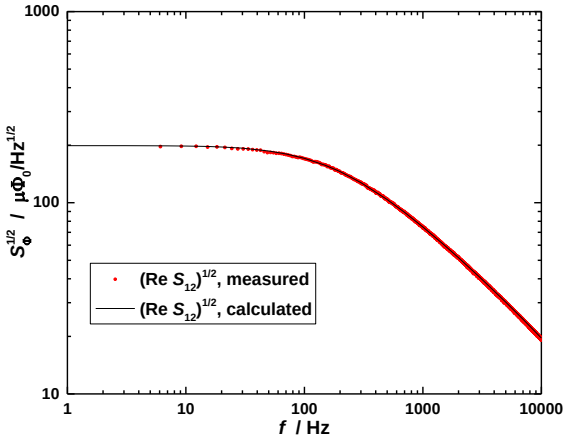

Figure 4. Flux noise referring to the SQUIDs at 4.23 K with temperature sensor. $N \approx 12200$ for experimental CPSD data.

3.2. Temperature measurements

To demonstrate the applicability of the concept, first test measurements with the pMFFT operated in secondary mode have been carried out in the temperature range from 4.2 K to 9 mK. In secondary mode the realization of only one precisely known reference temperature T_{Ref} is needed at which a so-called calibration spectrum $S_{12}(f,T_{\mathrm{Ref}})$ is acquired for the TMFN. The unknown temperature one is interested in is then obtained by averaging the ratio of the CPSDs over all frequency bins:

$$T = T_{\mathrm{Ref}} \left\langle \frac{\mathrm{Re}(S_{12}(f,T))}{\mathrm{Re}(S_{12}(f,T_{\mathrm{Ref}}))} \right\rangle . \tag{7}$$

This equation was evaluated using an improved non-parametric estimation according to [14] for frequencies up to 1 kHz, although the usable correlation bandwidth [8] was much larger. The reference temperatures T_{2000} were provided by a MFFT calibrated according to the PLTS-2000 with a relative uncertainty of $4 \cdot 10^{-4}$. The calibration of the pMFFT using the MFFT was carried out at $T_{\mathrm{Ref}} = 0.478$ K.

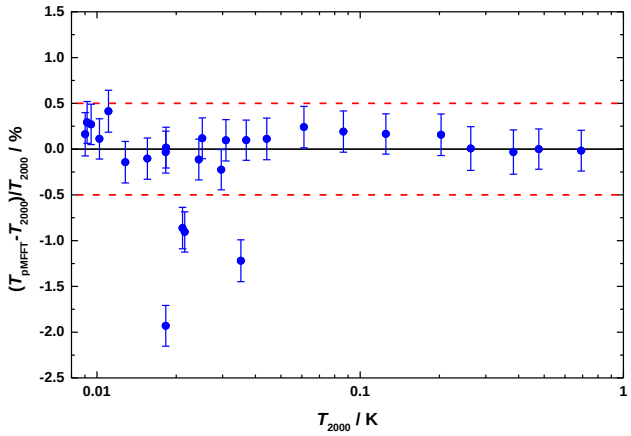

Figure 5. Relative deviations of the temperature values measured with the pMFFT in secondary mode from a copy of the PLTS-2000. Error bars indicate the relative uncertainty for a coverage factor $k = 2$. The red dashed lines mark the ±0.5% deviation range.

Figure 5 shows the relative deviations of the temperature readings of the pMFFT from the reference thermometer. Most of the data points are well within a ±0.5% interval having a typical relative uncertainty of 0.25% ($k = 2$) dominated by the uncertainty of T_{Ref} and the statistical uncertainty. From the good agreement between the pMFFT and the reference thermometer we conclude that the influence of non-thermal magnetic flux noise present in both thermometers in different forms is negligible in the investigated temperature range. This is because the pMFFT results

are based on a cross-correlation measurement whereas the reference thermometer values are based on a single-channel PSD. For the temperature sensor material of both the pMFFT and the reference thermometer, high purity copper containing only negligible amount of magnetic impurities was used from different batches purchased from the same supplier [13] within a few years. As no significant deviation in temperatures is visible over almost three decades of temperature we conclude that the influence of residual magnetic impurities in the sensor materials is negligible and the electrical conductivity for the copper used can be assumed to be in residual resistance limit and constant. Four data points fall below T_{2000} by more than 0.5%. Although the reason for that deviation is not yet clear, these points were identified as outliers by an abnormal single-channel noise in both channels.

4. Conclusions

We have developed and successfully tested the prototype of a calculable MFFT designed for primary thermometry at low temperatures. The new pMFFT utilizes a cross-correlation technique for the readout of the TMFN signals. The two SQUID channels are virtually independent from each other due to a special layout of the planar thin-film detection coils that minimizes the mutual induction and because the FLL feedback is applied into the detection coils. The magnetic flux measurements agree well with analytical calculations for the set-up. First measurements in the temperature range from 9 mK to 4.2 K in secondary mode of operation showed an excellent agreement within 0.5% with a reference thermometer carrying a copy of the PLTS-2000.

As a next step the calibration coil will be integrated in the pMFFT. This will enable us to operate the pMFFT in primary mode and to calculate thermodynamic temperature values directly from the measured TMFN. The pMFFT will finally contribute to resolve the long-standing discrepancies in the background data of the PLTS-2000 [15].

Acknowledgments

The research reported here was carried out within the EURAMET project “InK – Implementing the new kelvin” [15] and funding is kindly acknowledged from the European Community’s 7th Framework Programme, ERA-NET Plus, (Grant Agreement No. 217257).

References

[1] White D R, Galleano R, Actis A, Brixy H, De Groot M, Dubbeldam J, Reesink A, Edler F, Sakurai H, Shepard R and Gallop J 1996 *Metrologia* **33(4)** 325
[2] Netsch A, Hassinger E, Enss C and Fleischmann A 2005 *AIP Conf. Proc.* vol 850 p 1593
[3] Harding J T and Zimmerman E 1968 *Phys. Lett.* **27A N10** 670
[4] Rothfuß D, Reiser A, Fleischmann A and Enss C 2013 *Appl. Phys. Lett.* **103** 052605
[5] Beyer J, Drung D, Kirste A, Engert J, Netsch A, Fleischmann A, Enss C 2007 *IEEE Trans. Appl. Supercond.* vol. 17, issue 2, part 1, p 760
[6] Engert J, Beyer J, Drung D, Kirste A, Heyer D, Fleischmann A, Enss C and Barthelmess H-J 2009 *Journal of Physics: Conference Series* **150** 012012
[7] Beyer J, Schmidt M, Engert J, AliValiollahi S, Barthelmess H J, 2013 *Supercond. Sci. Technol.* **26** 065010
[8] White D R, Benz S P, Labenski J R, Nam S W, Qu J F, Rogally H and Tew W L 2008 *Metrologia* **45** 395
[9] Drung D, Aßmann C, Beyer J, Kirste A, Peters M, Ruede F and Schurig T 2007 *IEEE Trans. Appl. Supercond.* vol. 17, issue 2, part 1, p 699
[10] Kirste A, Drung D, Beyer J and Schurig T 2008 *J. Phys.: Conf. Ser.* **97** 012320
[11] Rajotte R J and Drouet M G 1975 *IEEE Trans. Power Appar. Syst.* **PAS-94** 89
[12] Sakakibara T, Goto T and Miura N 1989 *Rev. Sci. Instrum.* **60(3)** 444
[13] MaTecK GmbH, Im Langenbroich 20, D-52428 Jülich, Germany
[14] Wübbeler G and Elster C 2013 *Meas. Sci. Technol.* **24** 115004
[15] http://projects.npl.co.uk/ink/